



Article

Analysis of Olive Detachment Force to Improve Olive Shaker Efficiency Through Branch Modeling

Giuseppe Macoretta ¹, Sofia Matilde Luglio ^{2,*}, Federico Conforti ¹, Michele Abruzzo ¹, Lorenzo Gagliardi ², Marco Fontanelli ² and Michele Raffaelli ²

¹ Department of Civil and Industrial Engineering, University of Pisa, Largo Lucio Lazzarino 2, 56122 Pisa, Italy; giuseppe.macoretta@unipi.it (G.M.); conforti.fede@gmail.com (F.C.); michele.abruzzo@ing.unipi.it (M.A.)

² Department of Agriculture, Food and Environment, University of Pisa, Via del Borghetto 80, 56124 Pisa, Italy; lorenzo.gagliardi@phd.unipi.it (L.G.); marco.fontanelli@unipi.it (M.F.); michele.raffaelli@unipi.it (M.R.)

* Correspondence: sofiamatilde.luglio@phd.unipi.it

Abstract: Mechanical shaking enables efficient harvesting of olives, especially in hilly regions where automated farming is not feasible. This study delves into branch and olive detachment modeling to enhance the efficiency of a hand-held branch shaker. Shaking time, forces, accelerations, olive detachment forces and harvesting efficiency were experimentally measured. The fruit maturity index affected the force needed to detach the olive, with the highest value for olives at the C0 stage of maturity (5.93 N). No difference emerged among the tested shaking times (6 s and 12 s), neither in terms of harvest efficiency (mean 81.17%) nor in terms of damage (rate of 5.30). Therefore, the lower time was considered the most appropriate. Multibody and a Finite Element (FE) models were developed to investigate the branch response and the olive detachment condition. The stresses predicted by the FE harmonic analysis (about 8 MPa), based on the excitation force and shaking frequency measured during the tests, was in line with the measured olive detachment forces (3 to 8 MPa). The shaking frequency and the average branch acceleration in proximity to the shaker hook were 15 Hz and 50m/s², respectively. Further studies could focus on the impact of the branch shaker on operator health, particularly risks from prolonged vibration exposure.

Keywords: branch modeling; olives; harvesting; detachment forces; hand-held branch shaker

Academic Editor: Joe Mari Maja

Received: 3 December 2024

Revised: 16 January 2025

Accepted: 21 January 2025

Published: 27 January 2025

Citation: Macoretta, G.; Luglio, S.M.; Conforti, F.; Abruzzo, M.; Gagliardi, L.; Fontanelli, M.; Raffaelli, M.

Analysis of Olive Detachment Force to Improve Olive Shaker Efficiency Through Branch Modeling.

AgriEngineering **2025**, *7*, 28.

<https://doi.org/10.3390/agriengineering7020028>

Copyright: © 2025 by the authors. Licensee MDPI, Basel, Switzerland. This article is an open access article distributed under the terms and conditions of the Creative Commons Attribution (CC BY) license (<https://creativecommons.org/licenses/by/4.0/>).

1. Introduction

The olive tree (*Olea europaea* L.) holds a central role in Mediterranean culture, being one of the region's most important crops. Olive orchards are key economic resources, play a significant role in shaping the landscape, and are crucial for the conservation of soil, local flora, and fauna [1].

One of the most important operations for olive growers, both from an economic and qualitative perspective, is harvesting. Olive harvesting is currently receiving renewed attention, with a focus on technologies to be implemented. Olive cultivation in the Mediterranean basin exemplifies the coexistence of various harvesting methods, ranging from narrow hedgerow orchards (with over 1500 trees ha⁻¹) suited for straddle harvesters to traditional orchards (17–300 trees ha⁻¹), where harvesting is still performed manually [2].

Traditional orchards are still very widespread. These types of orchards are usually established in dry-farmed areas, characterized by the formation of one or several trunks, inconsistent planting arrangement, and wide irregularly shaped canopy trees [3]. The mechanization of harvesting is difficult to perform, due to the plants' shape, the orography of the olive orchards, the small farm size, or the lack of resources [4]. Consequently, current commercial systems rely on solutions that are highly conditioned by manual requirements (i.e., long poles or sticks), making the harvesting process complex and expensive [5]. This manual method can be complemented by hand-held harvesting systems [6], boosting operator productivity to 30–50 kg per hour per person, compared to 15–25 kg per hour when using poling sticks for manual harvesting [7]. Among hand-held olive harvesters, hook-type harvesters (branch shakers) feature a hook at the top of a pole, which moves alternately due to the machine's engine, held by the operator. After the user grabs an olive branch with the hook, the shaker rapidly moves the branch with high frequency (10–20 Hz), allowing for fruit detachment [8–10]. When designing a branch shaker, it is essential to prioritize harvest efficiency while also minimizing damage to both the olive plants and the operator.

The core idea behind shaking harvesting is to deliver an appropriate amount of kinetic energy to the fruiting branches, creating a force that detaches the fruit from the stem. Fruit removal occurs when the applied force of detachment exceeds the tensile strength of the pedicel–fruit connection [11]. Harvesting ripe olives using vibration techniques relies on accurately determining vibration parameters such as frequency, amplitude, and duration [12]. Authors [13] have found that increasing either the vibration frequency or amplitude improves harvesting efficiency. It is important to consider that the kinetic energy imparted by the shaker to the main branch can be largely dissipated. This is due to the complex mechanisms of vibration transmission among the branches, the resistance of the leaves, and internal energy losses within the wood and the root/soil system [14,15]. Indeed, the vibrations created by the shaker are greatly diminished by aerodynamic drag from the foliage in the air, the interactions among side branches linked to the main limb, and the damping effects occurring within the stem and root system [16]. The position on the tree where hand-held systems are applied is also crucial for their effectiveness. Applying high levels of acceleration in areas near the fruit allows these systems to achieve high harvesting efficiency [10].

The olive–branch system dynamics were investigated in the recent literature [17], and simplified Finite Element (FE) models were developed to catch the dynamic response of the tree [18–22]. However, a complete investigation gathering data from experimental activities as well as analytical and numerical analyses to obtain a model able to provide a framework for the optimization of the branch shaker olive harvesting performance, while preserving the olive tree and operator's health, is still an open question. Most of the FE models presented in the scientific literature [21,22] do not integrate the geometry of the olive stem. However, as demonstrated by [17], stem bending plays a fundamental role and cannot be accurately captured by models that consider only the olive acceleration resulting from branch movement.

This study aims to provide a framework for understanding the dynamic response of olive branches and to assess whether the FE model can accurately capture the critical conditions for olive detachment in order to improve branch shaker harvest performance. In this regard, this study includes combined experimental measurements—including shaking forces, shaking time, accelerations, olive detachment forces, and harvesting efficiency—with analytical and numerical modeling of the branch–olive system.

2. Materials and Methods

2.1. Analytical Branch Modeling

Harvesting of fruits performed by vibrational mechanisms is based on their detachment caused by dynamic inertial forces. After reaching steady-state conditions, a shaker attached to a branch (or the whole tree) produces a sinusoidal acceleration that provides the driving force for the fruits' detachment. In the present model, only the branch shaking is considered, and the fruits are accelerated by the dynamic response of the branch. An external force (F_h) with variable amplitude and frequency, depending on the mechanisms used, is applied on the branch at a distance (l_h) from the trunk.

Despite the mechanism chosen, a first-order model of the branch can be devised by considering it as a cantilever beam fixed on the trunk with a concentrated mass at its tip, representing olives, leaves, and twigs, as shown in Figure 1. The elasticity and damping, as well as the branch mass, are modeled with the cantilever beam mechanical properties.

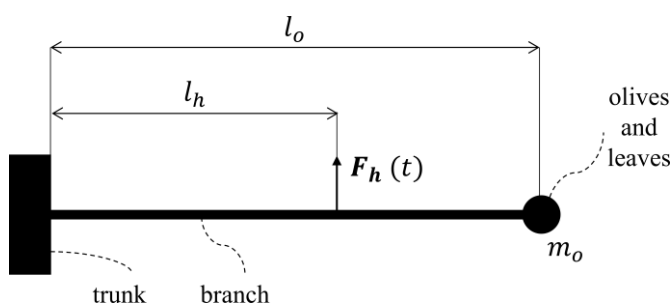


Figure 1. Beam model of the branch.

However, to write the dynamic response of the system, the branch can be considered as a rigid rod, and the stiffness and global damping can be explicated as a rotational spring and damper applied between the branch and the trunk. The global damping parameter includes the effects produced by the branch damping, friction with the surrounding branches, and aerodynamic drag on the leaves. The fixed constraint between the branch and the trunk, thus, becomes a frictionless hinge. For the sake of simplicity, in the present work, only the in-plane motion of the branch will be considered. Hence, the equivalent system shown in Figure 2, composed of a rigid beam with a rotational hinge connecting to the frame, can be defined. The only degree of freedom is the rotation of the branch with respect to the trunk, θ .

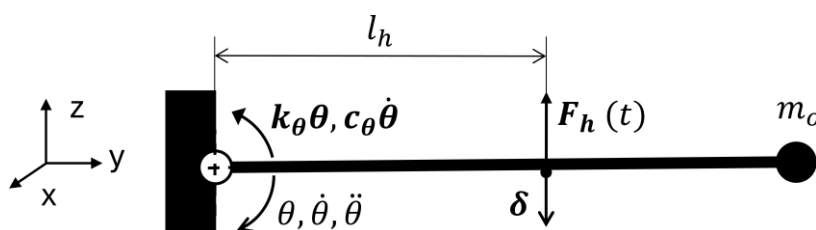


Figure 2. Equivalent model of branch. Full tip arrows are used for actions, while hollow tip arrows represent linear/rotational displacements and their time derivatives.

The external variable force F_h applied to the beam (branch) generates a dynamic displacement of the system and, consequently, the concentrated mass. Writing the dynamic equation of the system leads to:

$$I\ddot{\theta} = F_h L_p - k_\theta \theta - c_\theta \dot{\theta} \tag{1}$$

where I is the branch rotational inertia, k_θ is the stiffness of the rotational spring, c_θ is the damping of the equivalent rotational damper. In the equation, the influence of

gravitational force on the dynamic behavior of the system was omitted, as it impacts only on the static equilibrium conditions of the system and not on its dynamics. It was assumed that the shaking mechanism did not produce any frictional force on the branch and that its action was orthogonal to the force application region during the beam deflection, due to the small stroke of the common branch shaking mechanisms. Furthermore, no backlash was assumed on the branch gripping.

The stiffness (k_θ) is defined by equating the deflection of the external force application point on the rigid rod and the deflection of the same point of the cantilever beam, δ , when subjected to a concentrated load, F_h , at a distance l_h from the fixed constraint. Only the portion of the cantilever beam between the trunk and the force application point plays a role in the branch stiffness. The deflection of the cantilever beam in those conditions is:

$$\delta = \frac{F_h l_h^3}{3 E_b J_b} \tag{2}$$

where the geometrical and elastic proprieties of the branch are represented, respectively, with J_b the inertial moment of the branch section, and E_b the Young's modulus of the olive wood.

As the rotation of the rigid rod is

$$\delta = l_h \theta \tag{3}$$

and it is linked to the torque applied by the external force

$$k_\theta = \frac{F_h l_h}{\theta} \tag{4}$$

the rotational spring constant becomes:

$$k_\theta = \frac{F_h}{\delta} l_h^2 = \frac{3 E_b J_b}{l_h^3} \tag{5}$$

The damping ratio can be calculated using the logarithmic decrement method [21] by experimentally measuring the decreasing amplitude of n consecutive free oscillations. This method leads to a first approximation of the damping ratio due to wood damping and aerodynamic forces on the branch leaves, independent of the shaking speed of the branch. As a result, the damping ratio ζ was calculated using the following equation:

$$\zeta = \frac{\delta_n}{2\pi n} = \frac{\ln\left(\frac{x_1}{x_n + 1}\right)}{2\pi n} \tag{6}$$

Experimental observations were carried out on 5 trees with similar branches, applying a static displacement equal to the shaking mechanism stroke and measuring the oscillation amplitude decrement after 5 consecutive free oscillations. As the mean result of those experiments, $\zeta = 0.1$ was found. The branch damping factor can be assumed to be isotropic [22]. Having calculated ζ , the rotational damping constant can be evaluated as:

$$c_\theta = 2 \zeta \sqrt{k_\theta I} \tag{7}$$

2.2. FE Branch and Olive Stem Modeling

The branch dynamic response can be described in more detail by setting up an FE model.

A simplified branch, shown in Figure 3, was modeled as a variable section cylinder, which presents a stem and an olive at its end. It is a simplified model that neglects all the shape and curvature variations intrinsically present in a real branch, as well as the branch bifurcations and twigs. A cylindrical olive stem and an olive were introduced at the branch tip. The weight of the remaining olives was introduced as a concentrated mass

connected to the branch end. The branch dimensions are reported in Figure 3. The model is based on the average dimensions of the branches that were experimentally tested. The diameter of the cylinder that represents the olive stem, 1.2 mm, is the average value measured from more than 20 olive stems among the investigated olives (Section 2.4.1).

The branch geometry was severely simplified as it is aimed at capturing the first-order results in terms of dynamic branch response and olive detachment condition. A more detailed geometry, based on an extensive sensitivity analysis and experimental measurements, will be necessary to improve the accuracy of the predictions.

The branch body was modeled as an orthotropic linear elastic homogeneous body, considering the stiffness matrix obtained by [23] (Young's modulus along the branch axis direction 14.8 GPa). The olive stem was modeled as an isotropic linear elastic body, whose stiffness was evaluated via the measurement of its deflection when subjected to a controlled load applied in the olive connection point. Based on that hypothesis, a stem stiffness equal to 0.1 GPa can be assumed.

The density of the branch and stem bodies was assumed equal to the average olive wood density derived from the scientific literature (1100 kg/m^3) [22,24].

The olive was modeled as a flexible body, having a density based on the results of the experimental campaign detailed in Section 3.1. The olive stiffness, although negligible for the aim of the model, was assumed equal to the stem stiffness.

The model was meshed with 3D 5-node tetrahedral elements, having 3 DOF per node. The model featured 85,000 elements. The model was solved in Ansys Mechanical for obtaining the natural frequencies of the branch and its harmonic response during the shaking. A modal superposition (MSUP) approach was adopted. A modal analysis was performed to determine the natural frequencies and the corresponding modal shapes, followed by a harmonic analysis.

The harmonic analysis was set up considering the shaking force that was measured during the experimental tests carried out on branches having a similar stiffness and the damping ratio evaluated via the logarithmic decrement method. A global damping equal to the damping ratio evaluated by the logarithmic decrement method was applied.

Both in the modal and harmonic analysis, a null displacement was imposed on each node of the right end of the branch cylinder, Figure 3, to model the connection with the tree trunk, which was considered as a fixed constraint. The internal olive–stem and stem–branch connections were modeled as bonded contacts between separate bodies.

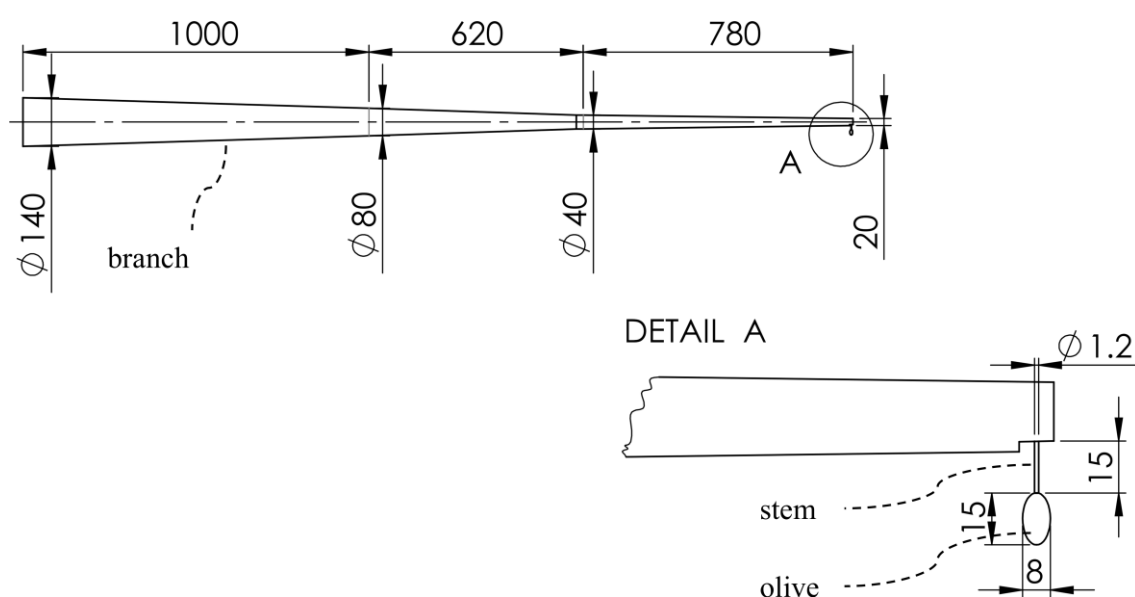


Figure 3. Dimensions of the branch considered in the FE model . Dimensions in mm.

2.3. Olive Detachment Modeling

The branch shaking produces the olive detachment because of the inertial forces acting on the olive, which can be modeled as the mass of an accelerated pendulum. The olive is subject to the superposition of the acceleration of the branch, measured in the branch–stem connection point and the acceleration deriving from the motion of the pendulum represented by the stem–olive system. In other words, the stem–olive pendulum is excited as a consequence of the branch motion.

Following the assumption made for the branch modeling, a 2D model is considered for the olive–stem system, taking into account only the oscillation within a plane containing the branch and shaking force directions.

A first-order model can be devised by neglecting the stem stiffness and damping, as the resultant forces can be assumed to be significantly lower than the inertial forces. Hence, the connection between the stem and the branch can be modeled as a frictionless hinge, as shown in Figure 4.

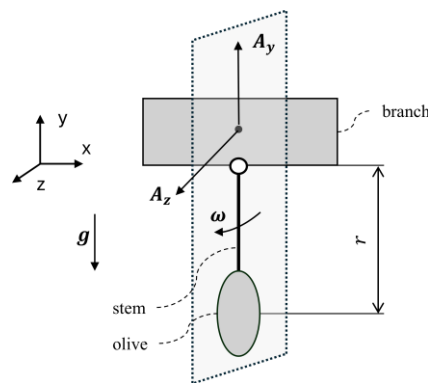


Figure 4. Olive pendulum model in vertical position under the branch. Dotted box represent the olive motion plane.

Considering the stem and olive as a pendulum oscillating under the branch, the dynamic equation of the system can be written, assuming the small oscillation approximation:

$$\ddot{\theta}_o - \frac{g}{r} \theta_o = 0 \tag{8}$$

where θ_o is the angular coordinate describing the olive motion and r the pendulum length.

The position and velocity equation of olive oscillation can be obtained; thus, adding the acceleration of the branch in the revolute joint coordinate, the dynamic inertial force of the olive can be written as (7):

$$F_i = m_o a_o \tag{9}$$

where the acceleration acting on the olive can be written as (8):

$$a_o = A_z \sin \theta + A_y \cos \theta + m_o r (\omega_z^2 + \omega_x^2) + g \cos \theta \tag{10}$$

where a_o is the total olive acceleration, A_z and A_y the branch accelerations in proximity to the stem, m_o the olive mass, r the stem length, ω_z and ω_x the rotational velocity of the pendulum, and g the gravitational acceleration.

However, to better understand the olive dynamics, a more detailed model considering the olive stem stiffness and damping has to be implemented. As presented in Section 2.1 for the branch model, the stem stiffness and damping were implemented as equivalent torsional forces applied on the frictionless hinge, representing the connection between the stem and the branch.

The whole branch–olive system can be, thus, described using a multibody model, shown in Figure 5, composed of two rigid beams, representing, respectively, the branch and the stem. Two revolute joints connect the branch to the trunk, which acts as a frame, and the stem to the branch. By employing the approach introduced in Section 2.1 and considering the branch and stem mechanical properties introduced in Section 2.2, the torsional spring stiffness and the torsional damping coefficient have been imposed as equal to $2.6 \cdot 10^4 \text{ N m/rad}$ and 220 N m/(rad/s) for the frame–branch connection and 2 N mm/rad and $0.01 \text{ N mm/(rad/s)}$ for the branch–stem connection, respectively.

The olive detachment condition depends on the inertial force produced by the olive acceleration and on the relative position between the olive and the stem connection point on the branch, which determines the stresses present in the stem. The FE model provides a more accurate analysis of the critical conditions leading to olive detachment and the associated stress distribution.

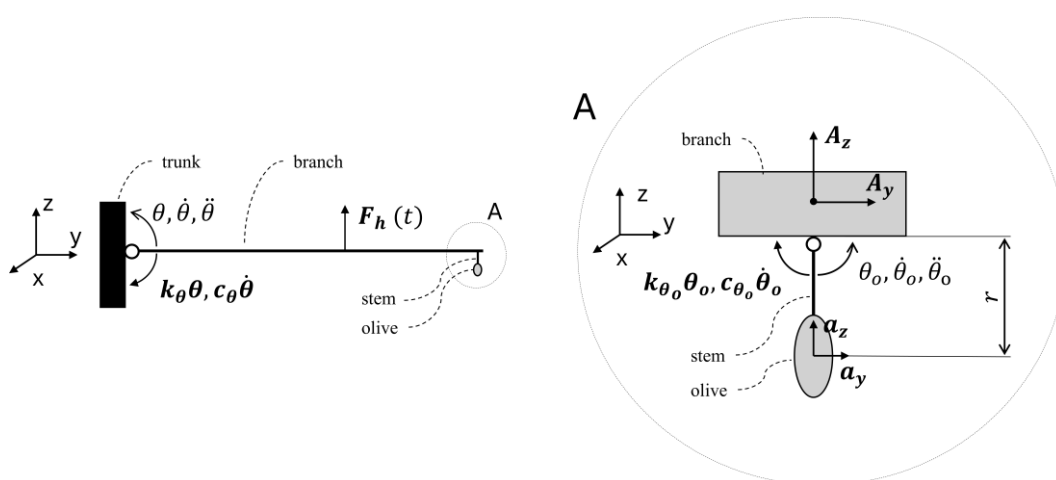


Figure 5. Olive–stem subsystem. The reference system is fixed to the frame.

The multibody model was implemented in the Matlab R2023a Simscape® solver, Figure 6. The external mechanical excitation was modeled as a sinusoidal force orthogonal to the axis of the branch beam by introducing a specific reference system located in the shaking force application point. The amplitude and frequency of the force were selected based on the value measured in the experimental tests.

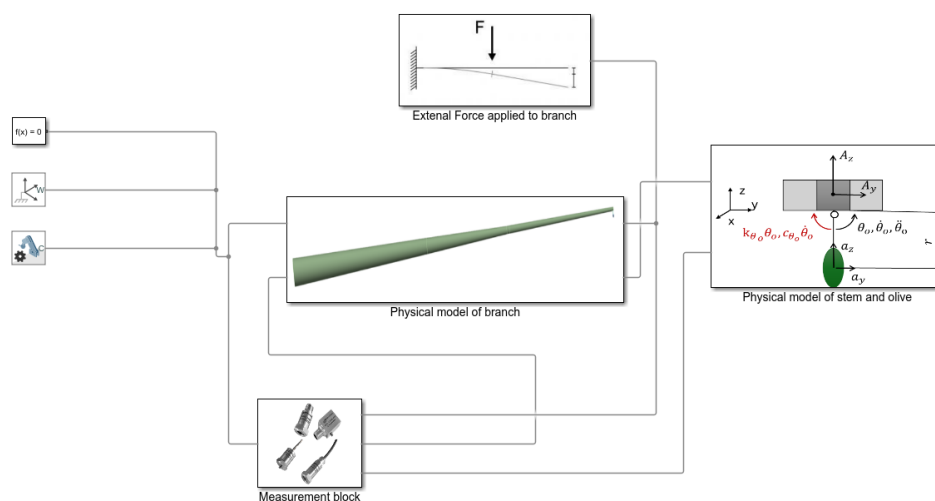


Figure 6. Simscape (MATLAB) multibody numerical model.

2.4. Experimental Trial in Olive Orchards

2.4.1. Olive Orchard Characterization

The trial was conducted in a rainfed and terraced olive orchard located in San Giuliano Terme (PI, 43°45'04.2" N, 10°28'21.4" E). The plants, cultivar Leccino, were managed using a multi-branched vase pruning system (polyconic). The average yield per plant over the years is around 6.5 kg. Before starting the trial, tree characterization was conducted, and tree sizes were manually measured using the metric system and a range rod [25]. The geometry of the trees was established by measuring the tree height and the canopy dimension. The canopy was characterized by measuring the overall canopy height above the ground level (m), the height from the ground to the canopy skirt (m), the canopy width high (m) and the canopy width low (m) [25]. The mean values with the corresponding standard deviation are reported in Table 1.

Table 1. Dimensional characterization of trees' structure (mean \pm standard deviation).

Trees Parameters	
Tree height (m)	4.32 \pm 0.14
Canopy width high (m)	4.09 \pm 0.42
Canopy width low (m)	3.60 \pm 0.40
Canopy skirt height (m)	1.00 \pm 0.18

After assessing the uniformity of the plants within the olive orchard, three plants were randomly selected, and 25 fruits were randomly taken from each tree. They were detached with a dynamometer tension force gauge (Correx, Haag-Streit, Switzerland), weighed with a digital precision scale (max capacity of 3×10^3 g, minimum capacity of 5×10^{-2} g), and their maturity index (Jaen index) was analyzed by sight according to the method described in [25]. Following the procedure described by García et al. [26], a subjective evaluation of the detached olives' skin and flesh was conducted to divide them into different groups (from group 0 for skin bright green to group 7 for skin black with 100% purple flesh).

2.4.2. Olive Shaking Efficiency and Damage Assessment

A prototype shaking device was provided by AgreeCrop s.r.l. (Pisa, Italy). It is a hand-held branch shaker with a fixed hook that can grasp a 40 mm diameter branch.

The olive shaking efficiency and the damage evaluation were conducted at the end of each harvesting test. Olive harvesting nets were laid out at the beginning of each test to collect fruits. There were no fruits falling outside the nets. The fruits that remained attached to the branch after the shaking activity were collected manually and weighed. The olive shaking efficiency was evaluated as the harvest efficiency, reported by Sola-Guirado et al. [25], using Equation (11):

$$\text{Harvest Efficiency (\%)} = \frac{\text{Fruit harvested}}{\text{Fruit non detached} + \text{Fruit harvested} + \text{Fruit fallen on the ground}} \times 100 \quad (11)$$

No fruits fell on the ground, because the net managed to collect them. The amount of machine damage was also quantified by collecting and weighing leaves, twigs, and branches (the debris). The damage was quantified on 100 g of fruits harvested following the formula reported by Sola-Guirado et al. [25] (12):

$$\text{Damage} = \frac{\text{debris (kg)}}{100 \text{ kg of fruit harvested}} \quad (12)$$

No twigs or branches were broken during the shaking activity, so only the fallen leaves were considered. Both fruits and debris were weighed through the digital precision scale.

2.4.3. Statistical Analysis

Data analysis was carried out using the statistical software R version 4.3.2. The Shapiro–Wilk test and Bartlett test were performed to assess data normality and homoscedasticity, respectively. The data were transformed with a square root transformation, when necessary, to respect the normality assumption. Data regarding the olive shaking efficiency (%), damage, olive detachment force (N), and olive mass (g) were analyzed with the analysis of variance (ANOVA). The fruit maturity index was considered as a fixed factor with three levels (C0, C2, and C4), as well as the shaking time (12 s and 6 s). LSD post hoc test at 0.05 probability was carried out for the analysis of the fruit maturity index with the package “agricolae”.

2.4.4. Branch Accelerations and Force Measurement

Experimental measurements of the accelerations present on the different branch zones during the shaking by a hand-held portable shaker were carried out.

Triaxial analogic accelerometers (ADXL356, Analog Devices Inc., Norwood, MA, USA) were applied in proximity to the shaker–branch connection point, at half the distance between the shaker connection point and the trunk and in proximity to the branch end (at about 50 cm from the shaker connection point) (Figure 7). Their signals were acquired by using an Arduino Mega board and converted by using the specific accelerometer calibration values.

The shaking force was also measured by applying a pair of strain gauges on the rod connecting the shaking machine to the branch, adopting a half-Wheatstone bridge configuration to maximize the signal, considering a normal load on the rod (diagonal bridge configuration). The effective dimensions of the rod were considered, as well as its elastic modulus, to obtain the applied force. The force signal was synchronized with the accelerometer ones.

All the experimental signals were filtered using a band-pass filter implemented in MATLAB. The lower cutoff frequency was set at 5 Hz to filter out static noise, while the upper cutoff frequency was set at 40 Hz to include only the excitation frequency and its harmonics up to the 3rd order. The proposed band-pass filter allows for the exclusion of most noise present in the signals, including electrical noise (50 Hz and odd harmonics).



Figure 7. Triaxial accelerometer applied near the branch tip. Local accelerometer y -axis was aligned with the local branch axis.

3. Results

3.1. Field Trial Results

Three main maturity indices were identified from the fruit characterization analysis. The average weight and the average detachment force were measured for each maturation index detected. The results are reported in Table 2.

Table 2. Characterization of the fruits, including the average weight and the average detachment force expressed in gF and N, in relation to the maturity indices observed in the field.

Maturity Index	Mass (g)	Detachment Force (gF)	Detachment Force (N)
C0	1.35	605.10	5.93
C2	1.46	472.45	4.63
C4	1.47	374.49	3.67

Results of the analysis of variance regarding the effect of fruit maturity index on weight and detachment force are reported in Table 3. The highest force was applied to olives with a fruit maturity index C0 (5.93 N), followed by C2 (4.63 N) and C4 (3.67 N).

Table 3. ANOVA analysis results on the effect of fruit maturity index on weight and detachment force.

Source	Mass (g)	Detachment Force (N)
Fruit maturity index	NS	***

$p < 0.001$ “***”; NS: not significant.

The results of the one-way ANOVA regarding the effect of shaking times (6 s and 12 s) on harvest efficiency and damage are reported in Table 4.

Table 4. ANOVA analysis results on the effect of shaking time on harvest efficiency and damage.

Source	Harvest Efficiency	Damage
Shaking time	.	NS

$p < 0.1$ “.”; NS: not significant.

The diameter of the olive stem was measured as well, obtaining an average value of 1.2 ± 0.2 mm. The average ultimate strength of the stem wood, thus, ranged from 3 to 6 MPa, with a maximum value of 8 MPa.

3.2. Branch Acceleration Measurement

All the acquired data show a high signal-to-noise ratio. As shown in Figure 8, where the raw spectra of the accelerometers present on the branch are reported, the spectrum of the signals presents well-distinguishable frequency peaks corresponding to the actuation frequency of the shaker (15 Hz) plus first-order superharmonics (2 \times , 3 \times).

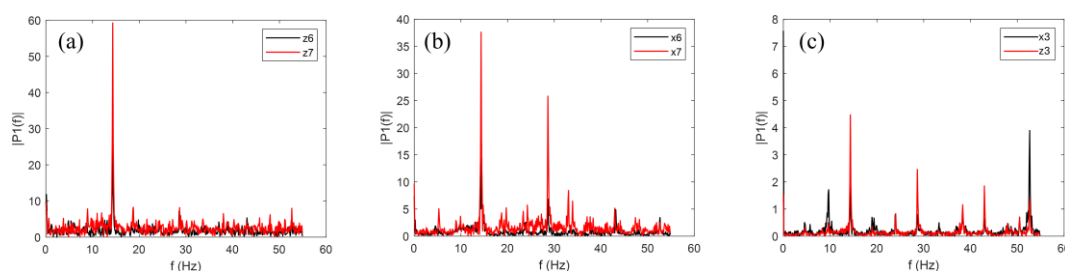


Figure 8. Accelerometer raw signal spectra for a representative case. Spectra of the accelerometers placed in proximity to the branch grasping (6) and nearest to the tip (7) regions in directions

orthogonal to the branch axis (a) and (b), signals orthogonal to the branch axis of the accelerometer placed in the middle between the trunk and the branch grasping region (c).

The modulus of the accelerations orthogonal to the branch axis, measured in proximity to the shaker–branch grasping point, at half the distance between the hook grasping point and the trunk and in proximity to the branch tip, is presented in Figure 9. The signals did not present a variation trend over the shaking duration (about 6 s). The data were preliminarily denoised and filtered with the 5–40 Hz band-pass filter before calculating the acceleration modulus.

The maximum value of the acceleration measured in the region nearest to the branch tip was greater than 150 m/s², while the average value was about 100 m/s². An average acceleration of 50 m/s² was measured in proximity to the shaker hook.

It can be observed that the average value of the branch acceleration grows monotonically from the trunk to the tip and that the average value of the accelerations measured in proximity to the branch tip is about two-times the value measured near the hook connection point. The acceleration growth while moving towards the branch tip is, thus, more than linear, suggesting that dynamic amplification due to the branch elasticity occurs.

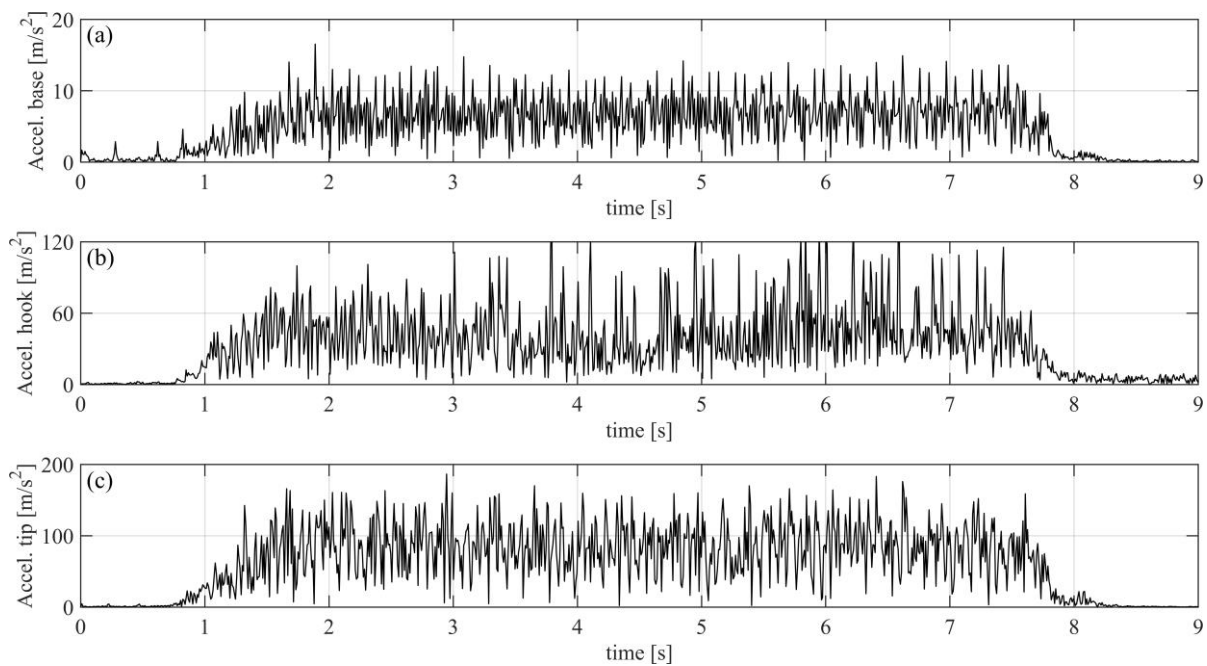


Figure 9. Modulus of the accelerations orthogonal to the branch axis, measured at half the distance between the hook grasping point and the trunk (a), in proximity to the shaker–branch grasping point (b) and in proximity to the branch tip (c).

3.3. Analytical Model Response

The olive acceleration predicted by the analytical model implemented in the MATLAB Simscape solver is shown in Figure 10. It can be observed that the olive acceleration along the horizontal direction (a_y) is significantly lower than the value in the vertical direction (a_z). The accelerations are in phase, and, thus, the resultant acting on the olive can be evaluated by considering the modulus of the two signals (13):

$$a_{tot} = \sqrt{a_y^2 + a_z^2} \tag{13}$$

The olive acceleration produces the inertial force (Equation (9)) that acts on the olive stem and leads to the olive detachment. Despite the lower contribution of horizontal acceleration, it can generate a significant flexural load on the stem.

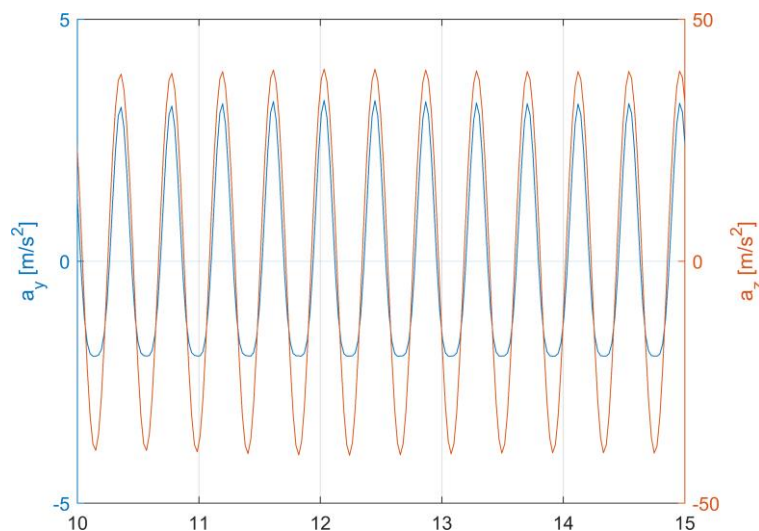


Figure 10. Absolute acceleration of the olive obtained by the multibody model in Simscape, along the horizontal (a_y) and vertical (a_z) directions. The axes are defined in Figure 5.

3.4. FE Model Predictions

3.4.1. Branch Dynamic Deformation

The shape of the modal response and the corresponding natural frequencies of the branch are reported in Table 5. The dynamic response is dominated by the oscillation of the olive around the branch–stem connection point and by the flexural deformation of the branch, with the former occurring at a lower frequency. For the first six modes, two modal shapes are present per each natural frequency due to the symmetry of the model.

Table 5. Modal shapes and natural frequencies for the first six modes.

Mode	Frequency, Hz	Brief Description
1.	8.4	Olive stem bending
2.	8.4	Olive stem bending
3.	11.5	Branch bending
4.	11.5	Branch bending
5.	40.2	High-order olive stem and branch bending
6.	40.2	High-order olive stem and branch bending

The deformed shape of the branch in shaking conditions was predicted by the harmonic analysis, following the MSUP approach. A sinusoidal force having the magnitude and the frequency of the average shaking force that was applied during the experimental campaign was applied. The model deformation is reported in Figure 11.



Figure 11. Predicted branch–stem deformation during shaking. Values in mm.

The harmonic analysis allowed us to investigate the effect of the shaking frequency, keeping the same shaking force and branch grasping point, on the dynamic response of the system.

As shown in Figures 12 and 13, a significant dynamic amplification of the acceleration on the branch end occurs when the excitation force is similar to the branch’s first flexural natural frequency. The value of the global damping ratio of the branch system affects the magnitude of the amplification and the frequency response.

A dynamic amplification factor (*DAF*) can be defined as the ratio of the olive and shaking point acceleration (14):

$$DAF = \frac{a_o}{a_{sp}} \tag{14}$$

where a_o is the magnitude of the acceleration of the olive center of mass, while a_{sp} is the magnitude of the acceleration of the shaking force application point on the branch. The *DAF* value as a function of the shaking frequency is reported in Figure 14 for damping ratios of 0.05 and 0.2. The experimental case, which presented a damping ratio of about 0.1, falls between these upper and lower boundaries.

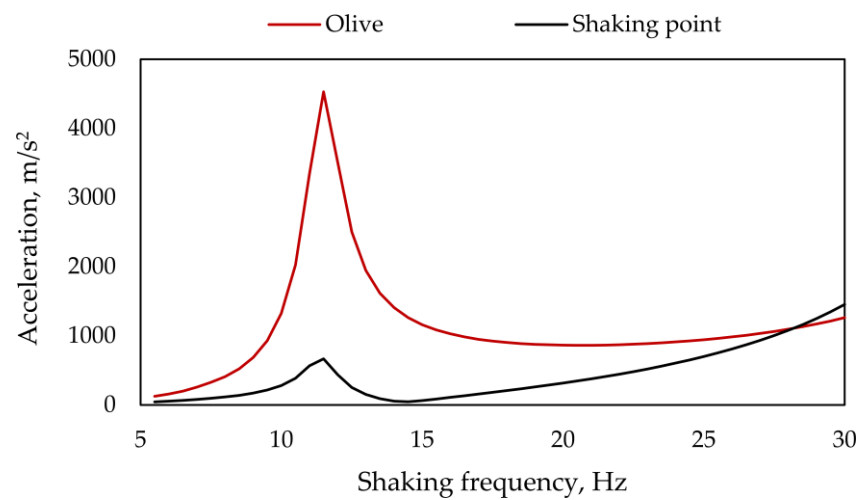


Figure 12. Magnitude of the acceleration of the node corresponding to the olive center of mass and of the shaking force application point, presented as a function of the shaking frequency. Damping ratio 0.05.

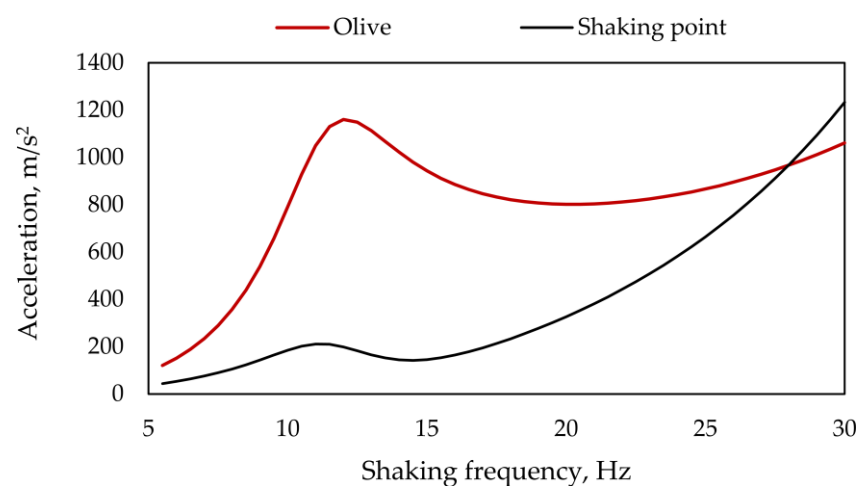


Figure 13. Magnitude of the acceleration of the node corresponding to the olive center of mass and of the shaking force application point, presented as a function of the shaking frequency. Damping ratio 0.2.

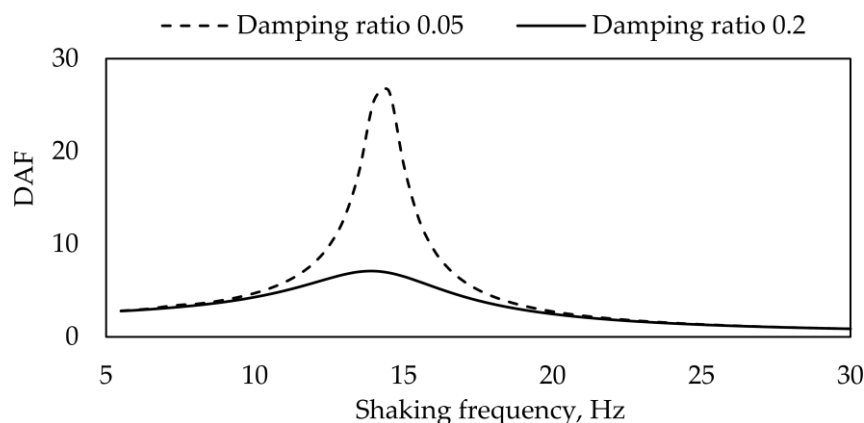


Figure 14. DAF value as a function of the shaking frequency for different damping ratios.

3.4.2. Olive Detachment Prediction

The FE model was solved by considering the shaking frequency adopted in the experimental campaign. The stem deformation and the stresses predicted in the stem critical region, namely the stem–branch connection, are reported in Figures 15 and 16. A global damping ratio of 0.1 was considered

The olive stem is subjected to a bending load due to the olive inertial forces, arising from the branch tip acceleration and olive oscillation with respect to the branch tip. The maximum stresses occurred in the stem–branch connection section, with the peak values in the region farthest from the section neutral axis. The stress state can, thus, be approximated by the response of a deformable cantilever beam loaded with a transverse force in proximity to the beam end.

The normal stress peak value was found to be 8.8 MPa, greater than the average ultimate strength of the stem wood obtained from the experimental tests (6 MPa).



Figure 15. Stress predicted by the harmonic analysis in the olive stem, evaluated at the shaking frequency. Values in MPa.

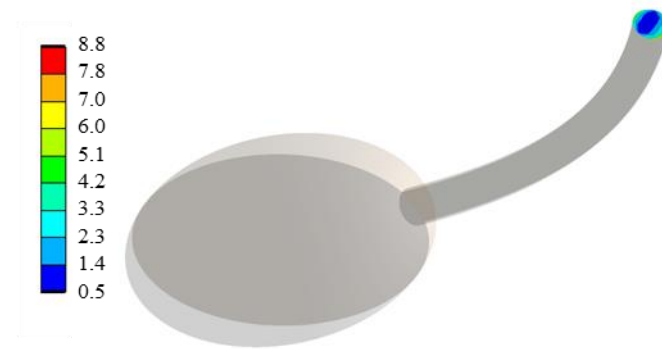


Figure 16. Detail of the equivalent Von Mises stress distribution on the critical region of the stem (the stem–branch connection), evaluated at the shaking frequency. Values in MPa.

The frequency response of the normal stress in the olive branch–stem connection section at various shaking frequencies is presented in Figure 17. The stress peak value and, thus, the most critical condition for the olive detachment occurs in proximity to the branch’s first flexural natural frequency (11.5 Hz), which is slightly lower than the applied shaking frequency (15 Hz). The maximum stress in the critical section varies from 3 MPa to 22 MPa as the shaking frequency changes from 6 to 30 Hz. The olive detachment is, thus, strongly affected by the machine shaking frequency.

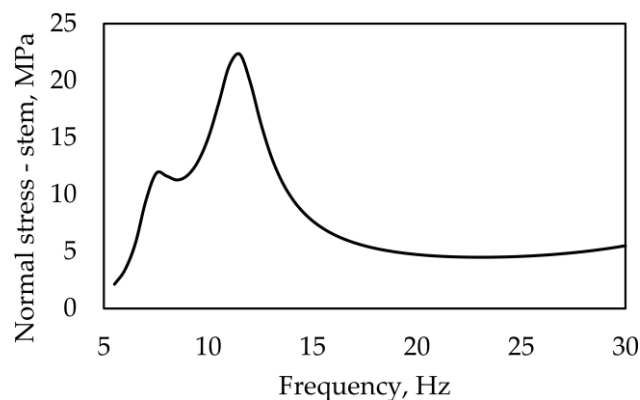


Figure 17. Frequency response of the maximum value of the normal stress along the olive stem at various shaking frequencies. Damping ratio 0.1.

4. Discussion

Concerning the fruit characterization, the presence of three main stages of maturity was detected (C0, C2, and C4). It was analyzed as fundamental information for identifying the optimal harvesting time, improving both the qualitative and quantitative characteristics of olive oil production [27]. In fact, according to [28], one of the main factors to monitor is the fruit detachment force, which, when it drops below 3 N, causes the fruit to fall and, consequently, the difficulty in recovering the latter during harvesting and a decline in the quality of the oil.

What emerged from this study is that the fruit maturity index ranged from C0 to C4, and it did not affect the olives’ mass, but it did affect the force needed to detach the olive, with the highest value for the olive in the C0 stage of maturity. This result is in accordance with [29], who obtained a decrease in resistance during the ripening process.

Furthermore, it was found that the shaking time (6 s and 12 s) did not affect the harvest efficiency. Shaking times longer than 6 s are not useful for increasing the harvesting efficiency, which resulted as 81.17% for both shanking times tested. It is an important result as it is fundamental to minimize the shaking time to limit the operator’s exposure to

vibrations that are harmful to the hand–arm system. These findings are in line with the findings of [30], which demonstrate that the establishment of a proper shaking time is fundamental to obtaining balanced harvesting efficiency. In fact, lengthening the shaking time can maximize the quantity of olives harvested per catch, but it reduces the quantity of olives harvested by each operator, without considering the damage to health [31]. As the typical vibration frequencies produced by commercial hand-held branch shakers fall within the most harmful range for the operator’s hand–arm system (EN ISO 5394), a possible reduction in the shaking durations significantly impacts the operator’s safety.

The damage rate caused by the branch shaker did not differ between the two shaking times. Both durations resulted in a damage rate of 5.30 in terms of debris production. Consequently, along with the efficiency results, it can be concluded that the lowest shaking time may be selected. In fact, according to [10], extending the harvest time led to high debris production, which has strong implications on the productive capacity of the olive trees.

The maximum value of the acceleration measured in the region nearest to the branch tip was greater than 150 m/s^2 , while the average value was about 100 m/s^2 . Despite the variability in the tree and the different frequency of the shaker (16.6 against 15 Hz), those values are in line with what has been observed in the recent literature [10].

The analysis of the branches’ structure and the comprehension of its dynamic response during the shaking are fundamental to optimizing olive harvesting because the shaking time within the same crop can vary according to the different points of vibration application [10,32,33]. In this regard, the proposed multibody model can be used to model a wide range of different branches. This model allows simply varying the principal parameters of the model, such as the length of the branch and stem, their stiffness and damping behavior, or the mass of the fruit [34]. However, multibody models cannot completely model the olive detachment condition, which is governed by the branch acceleration and the olive stem bending [17]. The olive detachment condition depends on the inertial force produced by the olive acceleration and on the relative position between the olive and the stem connection point on the branch, which determines the stresses present in the stem. Furthermore, a simplified multibody model does not consider the branch dynamic amplification, which affects the olive acceleration. An FE model is necessary to properly catch the dynamic response of the olive and the critical detachment condition.

In accordance with [22,29,34], the proposed FE model caught the influence of the dynamic vibration of the acceleration caused by the branch elasticity. The fundamental parameter for the optimization of olive harvesting via a hand-held portable shaker is the dynamic amplification of the acceleration applied by the device (the *DAF* value), which is presented in Figures 12–14, as a function of the shaking frequency. It focuses on an aspect that is not taken into account when a shaking force is applied by a device fixed on the branch [21] or by the trunk shaking [19,35]. Despite the branch geometry and mechanical properties (damping and stiffness) significantly affecting the value of the branch flexural natural frequency and the *DAF*–shaking frequency function, the dynamic amplification of the branch acceleration governs the acceleration transmitted from the branch shaker to the olive.

The damping coefficient used in the harmonic analysis was higher than the value reported by Sola-Guirado et al. [22] as it accounts for the global damping of the branch, including friction with surrounding branches. As shown in Figure 14, a higher *DAF* is obtained at the branch’s natural frequency when a damping ratio of 0.05 is used, which is consistent with the findings in [21].

Unlike previous studies [21,22] that did not incorporate olive–stem geometry in their FE models, the proposed approach integrates olive dynamics, providing insights into the mechanisms of olive detachment, as introduced by the analytical approach presented in

[17]. The model revealed that stem bending, caused by the inertial forces arising from the branch tip acceleration and the olive oscillation with respect to the branch tip, is the critical condition for olive detachment. This happens when the olive is at one extreme of its oscillation around the stem–branch connection point.

Although the local geometry of the stem–branch connection is not included in the model, the stresses predicted by the harmonic analysis, based on the excitation force and shaking frequency measured during the tests, were found to be in line with the measured olive detachment forces. The peak stress in the critical section was 8.8 MPa, exceeding the measured average strength of the olive–stem connection. These results are consistent with those obtained by [21], which considered an olive stem with a diameter of 1.5 mm.

Figure 17 shows that the maximum stress in the critical section is strongly affected by the machine shaking frequency, which can be tuned to facilitate the olive detachment. It is worth noting that the value of the peak stress and its frequency depends on the geometry of the simplified branch model that was implemented.

Further investigations could focus on refining the model by including more detailed branch geometry and twigs, incorporating the twigs' mechanical properties determined by [22]. An extended branch geometrical characterization and olive detachment force measurement campaign will be necessary to improve and validate the proposed FE model. Moreover, it is crucial to assess the model's sensitivity to the variations among olive trees and cultivars. By adopting this approach, a robust model can be defined, which is essential for optimizing the shaking frequency and minimizing the operator's exposure to harmful vibrations.

5. Conclusions

This study provided valuable insights for improving the harvesting performance in olive cultivation through a branch shaker. Among the findings derived from the field experiments, it emerged that the olive maturity index significantly influences the detachment force, confirming the importance of this factor in determining the optimal harvesting time.

The results showed that the longer shaking time did not increase damage to the olive trees but also did not improve harvesting efficiency. This indicates that shorter shaking times (6 s) can be employed as the optimal solution to reduce the operator exposure to the shaker vibrations.

The FE model revealed that the branch dynamic amplification governs the accelerations transmitted to the olive. Furthermore, it showed that the critical condition leading to olive detachment is the olive stem bending. The stress predicted by the harmonic analysis (peak value 8.8 MPa) was found to be in line with the measured olive detachment forces.

Such findings are essential to optimize not only the machinery design but also the operators' working conditions, while minimizing the tree damage.

The present work lays the groundwork for an extensive FE model validation and sensitivity analysis to the mechanical and geometrical parameters that can be found across olive cultivars. This approach will provide machine designers with the data necessary to optimize the shaking frequency of hand-held portable shakers and trunk shakers.

In addition, further studies could focus on the impact of the branch shaker on operator health. In particular, the research could address the minimization of the shaking time for a wide range of cultivars and fruit maturity indices, impacting the potential risks associated with prolonged exposure to vibrations.

Author Contributions: Conceptualization, G.M. and S.M.L.; methodology, G.M., S.M.L., F.C. and M.A.; software, F.C., M.A. and S.M.L.; validation, G.M., M.R. and M.F.; formal analysis, F.C., S.M.L., M.A. and L.G.; investigation, G.M., F.C., M.A., S.M.L. and L.G.; resources, G.M. and M.R.; data curation, S.M.L. and G.M.; writing—original draft preparation, G.M., S.M.L., F.C. and L.G.; writing—review and editing, M.A., S.M.L. and L.G.; visualization, M.R., F.C. and M.F.; supervision, G.M. and M.R.; project administration, G.M. and M.R.; funding acquisition, G.M. All authors have read and agreed to the published version of the manuscript.

Funding: This research received no external funding.

Data Availability Statement: Dataset available on request from the authors.

Acknowledgments: The authors gratefully acknowledge Eng. Vladimir Nemich and AgreenCrop s.r.l. (Pisa, Italy) for the support in the experimental activities and for providing their hand-held branch shaker and acceleration measurement devices.

Conflicts of Interest: The authors declare no conflicts of interest.

References

1. Fekete, R.; Vincze, O.; Süveges, K.; Bak, H.; Malkócs, T.; Löki, V.; Urgyán, R.; Molnár, A. The role of olive groves in the conservation of Mediterranean orchids. *Glob. Ecol. Conserv.* **2023**, *44*, e02490. <https://doi.org/10.1016/j.gecco.2023.e02490>.
2. Vossen, P. Olive Oil: History, Production, and Characteristics of the World's Classic Oils. *HortScience* **2007**, *42*, 1093–1100. <https://doi.org/10.21273/HORTSCI.42.5.1093>.
3. Aragon-Rodriguez, F.; Dias, A.B.; Pinheiro, A.; Peça, J.; Dias, I.L.; Castro-Garcia, S. Assessment of a Side-Row Continuous Canopy Shaking Harvester and Its Adaptability to the Portuguese Cobrançosa Variety in High-Density Olive Orchards. *Sensors* **2023**, *23*, 1740. <https://doi.org/10.3390/s23031740>.
4. Sola-Guirado, R.R.; Bayano-Tejero, S.; Aragon-Rodriguez, F.; Peña, A.; Blanco-Roldan, G. Bruising pattern of table olives ('Manzanilla' and 'Hojiblanca' cultivars) caused by hand-held machine harvesting methods. *Biosyst. Eng.* **2022**, *215*, 188–202. <https://doi.org/10.1016/j.biosystemseng.2022.01.010>.
5. Sperandio, G.; Biocca, M.; Fedrizzi, M.; Toscano, P. Economic and technical features of different levels of mechanization in olive harvesting. *Chem. Eng. Trans.* **2017**, *58*, 853–858. <https://doi.org/10.3303/CET1758143>.
6. Ghonimy, M.I.; Ibrahim, M.M.; Ghaly, A.E.; Rahman, A.E. Performance evaluation of hand-held olive harvesters. *Agric. Eng. Int. CIGR J.* **2021**, *23*, 127–137.
7. Rallo, L.; Barranco, D.; Castro-García, S.; Connor, D.J.; Gómez Del Campo, M.; Rallo, P. High-Density Olive Plantations. In *Horticultural Reviews*, 1st ed.; Janick, J., Ed.; Wiley: New York, NY, USA, 2013; Volume 41, pp. 303–384. <https://doi.org/10.1002/9781118707418.ch07>.
8. Deboli, R.; Calvo, A.; Preti, C.; Inserillo, M. Design and test of a device for acceleration reproducibility of hand held olive harvesters. *Int. J. Ind. Ergon.* **2014**, *44*, 581–589. <https://doi.org/10.1016/j.ergon.2014.05.007>.
9. Castro-Garcia, S.; Farinelli, D.; Ferguson, L.; Gil-Ribes, J.A.; Famiani, F. Olive Harvesting. In *The Olive: Botany and Production*; Fabbri, A., Baldoni, L., Caruso, T., Famiani, F., Eds.; Cabi: Wallingford, UK, 2024.
10. Sola-Guirado, R.R.; Castro-García, S.; Blanco-Roldán, G.L.; Jiménez-Jiménez, F.; Castillo-Ruiz, F.J.; Gil-Ribes, J.A. Traditional olive tree response to oil olive harvesting technologies. *Biosyst. Eng.* **2014**, *118*, 186–193. <https://doi.org/10.1016/j.biosystemseng.2013.12.007>.
11. Ghonimy, M.; Ibrahim, M.M.; Helmy, H.S.; Alzoheiry, A. Power requirements for olive mechanical harvesting using trunk shaker. *Sci. Rep.* **2024**, *14*, 25585. <https://doi.org/10.1038/s41598-024-77571-8>.
12. Bernardi, B.; Falcone, G.; Stillitano, T.; Benalia, S.; Bacenetti, J.; De Luca, A.I. Harvesting system sustainability in Mediterranean olive cultivation: Other principal cultivar. *Sci. Total Environ.* **2021**, *766*, 142508. <https://doi.org/10.1016/j.scitotenv.2020.142508>.
13. Sola-Guirado, R.R.; Jimenez-Jimenez, F.; Blanco-Roldan, G.L.; Castro-Garcia, S.; Castillo-Ruiz, F.J.; Gil-Ribes, J.A. Vibration parameters assessment to develop a continuous lateral canopy shaker for mechanical harvesting of traditional olive trees. *Span. J. Agric. Res.* **2016**, *14*, e0204. <https://doi.org/10.5424/sjar/2016142-7909>.
14. Leone, A.; Romaniello, R.; Tamborrino, A.; Catalano, P.; Peri, G. Identification of Vibration Frequency, Acceleration, and Duration for Efficient Olive Harvesting Using a Trunk Shaker. *Trans. ASABE* **2015**, *58*, 19–26. <https://doi.org/10.13031/trans.58.10608>.

15. Ma, R.; Homayouni, T.; Toudeshki, A.; Ehsani, R.; Zhang, X. An Experimental Study and Mathematical Modeling of Vibration Transfer in Pistachio Trees Using an Inertia-Type Trunk Shaker and Field-Adapted Wireless Sensors. *Shock. Vib* **2022**, *2022*, 9966848. <https://doi.org/10.1155/2022/9966848>.
16. Sola-Guirado, R.R.; Bernardi, B.; Castro-García, S.; Blanco-Roldán, G.L.; Benalia, S.; Fazari, A.; Brescia, A.; Zimbalatti, G. Assessment of aerial and underground vibration transmission in mechanically trunk shaken olive trees. *J. Agric. Eng.* **2018**, *49*, 191–197. <https://doi.org/10.4081/jae.2018.788>.
17. Alzoheiry, A.; Ghonimy, M.; Abd El Rahman, E.; Abdelwahab, O.; Hassan, A. Improving olive mechanical harvesting using appropriate natural frequency. *J. Agric. Eng.* **2020**, *51*, 148–154. <https://doi.org/10.4081/jae.2020.1057>.
18. Tombesi, S.; Poni, S.; Palliotti, A.; Farinelli, D. Mechanical vibration transmission and harvesting effectiveness is affected by the presence of branch suckers in olive trees. *Biosyst. Eng.* **2017**, *158*, 1–9. <https://doi.org/10.1016/j.biosystemseng.2017.03.010>.
19. Hoshyarmanesh, H.; Dastgerdi, H.R.; Ghodsi, M.; Khandan, R.; Zareinia, K. Numerical and experimental vibration analysis of olive tree for optimal mechanized harvesting efficiency and productivity. *Comput. Electron. Agric.* **2017**, *132*, 34–48. <https://doi.org/10.1016/j.compag.2016.11.014>.
20. Zhang, X.; Niu, Z.; Deng, J.; Mu, H.; Cui, Y. Vibration simulation and experiment of three open-center shape olive trees. *Vib. Procedia* **2022**, *41*, 60–65. <https://doi.org/10.21595/vp.2022.22523>.
21. Niu, Z.; Xu, Z.; Deng, J.; Zhang, J.; Pan, S.; Mu, H. Optimal vibration parameters for olive harvesting from finite element analysis and vibration tests. *Biosyst. Eng.* **2022**, *215*, 228–238.
22. Sola-Guirado, R.R.; Luque-Mohedano, R.; Tombesi, S.; Blanco-Roldán, G. Effect of leaves in the dynamic response of olive tree branches and their computational model. *Comput. Electron. Agric.* **2022**, *203*, 107490.
23. Formato, A.; Ianniello, D.; Pellegrino, A.; Vilecco, F. Vibration-Based Experimental Identification of the Elastic Moduli Using Plate Specimens of the Olive Tree. *Machines* **2019**, *7*, 46. <https://doi.org/10.3390/machines7020046>.
24. Mammoliti, A.; Cataldo, M.F.; Papandrea, S.F.; Proto, A.R. Mechanical properties of branch and stem wood for two Mediterranean cultivars of olive tree. *J. Wood Sci.* **2024**, *70*, 40. <https://doi.org/10.1186/s10086-024-02153-1>.
25. Sola-Guirado, R.R.; Sánchez-Cachinero, P.; Blanco-Roldán, G. Simultaneous trunk and branch shaking in an over-the-row olive harvester. *Biosyst. Eng.* **2023**, *231*, 92–103. <https://doi.org/10.1016/j.biosystemseng.2023.06.005>.
26. García, J.M.; Gutiérrez, F.; Barrera, M.J.; Albi, M.A. Storage of Mill Olives on an Industrial Scale. *J. Agric. Food Chem.* **1996**, *44*, 590–593. <https://doi.org/10.1021/jf950479s>.
27. Guzmán, E.; Baeten, V.; Pierna, J.A.F.; García-Mesa, J.A. Determination of the olive maturity index of intact fruits using image analysis. *J. Food Sci. Technol.* **2015**, *52*, 1462–1470. <https://doi.org/10.1007/s13197-013-1123-7>.
28. Castillo-Ruiz, F.J.; Jiménez-Jiménez, F.; Blanco-Roldán, G.L.; Sola-Guirado, R.R.; Agüera-Vega, J.; Castro-García, S. Analysis of fruit and oil quantity and quality distribution in high-density olive trees in order to improve the mechanical harvesting process. *Span. J. Agric. Res.* **2015**, *13*, e0209. <https://doi.org/10.5424/sjar/2015132-6513>.
29. Castillo-Ruiz, F.J.; Tombesi, S.; Farinelli, D. Olive fruit detachment force against pulling and torsional stress. *Span. J. Agric. Res.* **2018**, *16*, e0202. <https://doi.org/10.5424/sjar/2018161-12269>.
30. Aiello, G.; Vallone, M.; Catania, P. Optimising the efficiency of olive harvesting considering operator safety. *Biosyst. Eng.* **2019**, *185*, 15–24. <https://doi.org/10.1016/j.biosystemseng.2019.02.016>.
31. Lombardo, S.; Sarri, D.; Corvo, L.; Vieri, M. Approaching to the fourth agricultural revolution: Analysis of needs for the profitable introduction of smart farming in rural areas. In Proceedings of the 8th International Conference on Information and Communication Technologies in Agriculture, Food and Environment, HAICTA 2017, Chania, Greece, 21–24 September 2017; Volume 2030, pp. 521–532.
32. Camposeo, S.; Vicino, F.; Vivaldi, G.A.; Pascuzzi, S. Re-shaping pruning improves the dynamic response of centuries-old olive trees to branch-shaker vibrations application. *Front. Plant Sci.* **2023**, *14*, 1155120. <https://doi.org/10.3389/fpls.2023.1155120>.
33. Kouraba, K.; Gil-Ribes, J.A.; Blanco-Roldán, G.L.; Jaime-Revuelta, M.A.; Barranco-Navero, D. Suitability of olive varieties for mechanical harvester shaking. *Olivae* **2004**, *101*, 39–43.
34. Hu, G.; Zhou, J.; Chen, Q.; Luo, T.; Li, P.; Chen, Y.; Zhang, S.; Chen, J. Effects of different picking patterns and sequences on the vibration of apples on the same branch. *Biosyst. Eng.* **2024**, *237*, 26–37. <https://doi.org/10.1016/j.biosystemseng.2023.11.010>.
35. Bentaher, H.; Haddar, M.; Fakhfakh, T.; Mâalej, A. Finite elements modeling of olive tree mechanical harvesting using different shakers. *Trees* **2013**, *27*, 1537–1545. <https://doi.org/10.1007/s00468-013-0902-0>.

Disclaimer/Publisher’s Note: The statements, opinions and data contained in all publications are solely those of the individual author(s) and contributor(s) and not of MDPI and/or the editor(s). MDPI and/or the editor(s) disclaim responsibility for any injury to people or property resulting from any ideas, methods, instructions or products referred to in the content.